GEOPHYSICS, VOL. 65, NO. 6 (NOVEMBER-DECEMBER 2000); P. 1803–1817, 5 FIGS., 1 TABLE.

Estimation of fracture parameters from reflection seismic data—Part II: Fractured models with orthorhombic symmetry

Andrey Bakulin*, Vladimir Grechka‡, and Ilya Tsvankin‡

ABSTRACT

Existing geophysical and geological data indicate that orthorhombic media with a horizontal symmetry plane should be rather common for naturally fractured reservoirs. Here, we consider two orthorhombic models: one that contains parallel vertical fractures embedded in a transversely isotropic background with a vertical symmetry axis (VTI medium) and the other formed by two orthogonal sets of rotationally invariant vertical fractures in a purely isotropic host rock.

Using the linear-slip theory, we obtain simple analytic expressions for the anisotropic coefficients of effective orthorhombic media. Under the assumptions of weak anisotropy of the background medium (for the first model) and small compliances of the fractures, all effective anisotropic parameters reduce to the sum of the background values and the parameters associated with each fracture set. For the model with a single fracture system, this result allows us to eliminate the influence of the VTI background by evaluating the differences between the anisotropic parameters defined in the vertical symmetry planes. Subsequently, the fracture weaknesses, which carry information about the density and content of the fracture network, can be estimated in the same way as for fracture-induced transverse isotropy with a horizontal symmetry axis (HTI media) examined in our previous paper (part I). The parameter estimation procedure can be based on the azimuthally dependent reflection traveltimes and prestack amplitudes of *P*-waves alone if an estimate of the ratio of the *P*- and *S*-wave vertical velocities is available. It is beneficial, however, to combine *P*-wave data with the vertical traveltimes, NMO velocities, or AVO gradients of mode-converted (*PS*) waves.

In each vertical symmetry plane of the model with two orthogonal fracture sets, the anisotropic parameters are largely governed by the weaknesses of the fractures orthogonal to this plane. For weak anisotropy, the fracture sets are essentially decoupled, and their parameters can be estimated by means of two independently performed HTI inversions. The input data for this model must include the vertical velocities (or reflector depth) to resolve the anisotropic coefficients in each vertical symmetry plane rather than just their differences.

We also discuss several criteria that can be used to distinguish between the models with one and two fracture sets. For example, the semimajor axis of the *P*-wave NMO ellipse and the polarization direction of the vertically traveling fast shear wave are always parallel to each other for a single system of fractures, but they may become orthogonal in the medium with two fracture sets.

INTRODUCTION

This is the second part of our series of three papers on characterization of naturally fractured reservoirs using surface seismic data. The main goal of the series is to provide a connection between fracture detection methods and rock physics models of fractured media, such as those developed by Hudson (1980, 1981, 1988), Schoenberg (1980, 1983), and Thomsen (1995). In particular, we are interested in elucidating the dependence of reflection seismic signatures on the physical properties of the fractures and in developing inversion algorithms for estimating fracture parameters using *P*-wave and converted (*PS*) reflection data.

In the first paper of the series (Bakulin et al., 2000; hereafter referred to as part I), we address these problems for transverse isotropy with a horizontal axis of symmetry (HTI media), which describes a single set of vertical, parallel, rotationally invariant fractures in a purely isotropic background medium. HTI is the

Manuscript received by the Editor April 20, 1999; revised manuscript received March 1, 2000.
*Formerly St. Petersburg State University, Department of Geophysics, St. Petersburg, Russia. Presently Schlumberger Cambridge Research, High Cross, Madingley Road, Cambridge, CB3 0EL, England. E-mail: bakulin@cambridge.scr.slb.com.
‡Colorado School of Mines, Center for Wave Phenomena, Department of Geophysics, Golden, Colorado 80401-1887. E-mail: vgrechka@dix.mines.edu; ilya@dix.mines.edu.

simplest azimuthally anisotropic model that provides valuable insights into the behavior of seismic signatures over fractured formations.

However, since the rock matrix usually exhibits some form of anisotropy, it is difficult to expect the HTI model to be adequate for typical fractured reservoirs. Here, we extend the approach of part I to more complicated, but likely more realistic, orthorhombic models. The description of seismic signatures in orthorhombic media can be simplified significantly by applying Tsvankin's (1997b) notation based on the analogy between the symmetry planes of orthorhombic and TI media. For instance, P-wave velocities and traveltimes are fully controlled by the P-wave vertical velocity and five dimensionless anisotropic coefficients, rather than by nine stiffnesses in the conventional notation. Also, this parameterization yields concise exact expressions for the NMO velocities of pure modes reflected from a horizontal interface (Grechka and Tsvankin, 1998).

As shown by Grechka et al. (1999), eight out of the nine parameters of orthorhombic media with a horizontal symmetry plane can be obtained from the NMO velocities of horizontal P- and split PS-events, provided the vertical velocities or reflector depth are known. Reflection moveout of P-waves alone is sufficient to find the orientation of the symmetry planes, the NMO velocities within them, and three anellipticity coefficients η. The parameters η, however, can be determined only if dipping events or nonhyperbolic moveout is available.

While orthorhombic symmetry may be caused by a variety of physical reasons, we restrict ourselves to two orthorhombic models believed to be most common for fractured reservoirs: (1) a single set of vertical cracks in a transversely isotropic background with a vertical symmetry axis (VTI) and (2) two systems of vertical fractures orthogonal to each other in an isotropic background medium. If the intrinsic anisotropy of the host rock and the anisotropy induced by the fractures are weak, the anisotropic coefficients of the background and fractures can be algebraically *added* in describing the effective medium. This result provides important insights into the influence of fractures on the effective anisotropy and helps to generalize the parameter estimation methodology of part I for orthorhombic media. For both orthorhombic models we relate Tsvankin's (1997b) anisotropic coefficients to the fracture compliances and introduce practical fracture characterization techniques operating with P- and PS-waves.

MODEL 1: ONE SET OF VERTICAL FRACTURES IN A VTI BACKGROUND

Effective orthorhombic medium

A single system of vertical fractures embedded in a VTI matrix yields an effective orthorhombic medium in which one of the symmetry planes coincides with the fracture plane. According to the linear-slip theory (Schoenberg, 1980, 1983), the effective compliance tensor of such a medium can be obtained by simply adding the excess fracture compliances to the compliance of the background. [Part I compares the linear-slip theory with the effective medium theories of Hudson (1980, 1981, 1988) and Thomsen (1995).] The inversion of the resulting compliance tensor yields the stiffness tensor (and the corresponding two-index stiffness matrix) of the fracture-induced orthorhombic model. If the fracture faces are perpendicular to the x_1-axis, the effective stiffness matrix $\mathbf{c}$ has the following form (Schoenberg and Helbig, 1997; Appendix A):

$$\mathbf{c} = \begin{pmatrix} c_{11} & c_{12} & c_{13} & 0 & 0 & 0 \\ c_{12} & c_{22} & c_{23} & 0 & 0 & 0 \\ c_{13} & c_{23} & c_{33} & 0 & 0 & 0 \\ 0 & 0 & 0 & c_{44} & 0 & 0 \\ 0 & 0 & 0 & 0 & c_{55} & 0 \\ 0 & 0 & 0 & 0 & 0 & c_{66} \end{pmatrix} = \left(\begin{array}{c|c} \tilde{\mathbf{c}}_1 & \mathbf{0} \\ \hline \mathbf{0} & \tilde{\mathbf{c}}_2 \end{array}\right), \quad (1)$$

where $\mathbf{0}$ is the 3×3 zero matrix and $\tilde{\mathbf{c}}_1$ and $\tilde{\mathbf{c}}_2$ are given by

$$\tilde{\mathbf{c}}_1 = \begin{pmatrix} c_{11_b}(1-\Delta_N) & c_{12_b}(1-\Delta_N) & c_{13_b}(1-\Delta_N) \\ c_{12_b}(1-\Delta_N) & c_{11_b} - \Delta_N \dfrac{c_{12_b}^2}{c_{11_b}} & c_{13_b}\left(1-\Delta_N \dfrac{c_{12_b}}{c_{11_b}}\right) \\ c_{13_b}(1-\Delta_N) & c_{13_b}\left(1-\Delta_N \dfrac{c_{12_b}}{c_{11_b}}\right) & c_{33_b} - \Delta_N \dfrac{c_{13_b}^2}{c_{11_b}} \end{pmatrix} \quad (2)$$

and

$$\tilde{\mathbf{c}}_2 = \begin{pmatrix} c_{44_b} & 0 & 0 \\ 0 & c_{44_b}(1-\Delta_V) & 0 \\ 0 & 0 & c_{66_b}(1-\Delta_H) \end{pmatrix}. \quad (3)$$

Here c_{ij_b} are the stiffness coefficients of the VTI background (constrained by $c_{12_b} = c_{11_b} - 2c_{66_b}$); Δ_N, Δ_V, and Δ_H are the dimensionless weaknesses of the fractures (Schoenberg and Helbig, 1997; Bakulin and Molotkov, 1998), which change from zero (no fractures) to unity (extreme fracturing). The tangential weaknesses Δ_V and Δ_H provide a measure of crack density, whereas the normal weakness Δ_N contains information about the fluid content of the fractures and possible fluid flow between the fractures and pore space (Schoenberg and Douma, 1988; part I).

Matrix (1) describes a special type of orthorhombic media with the stiffnesses satisfying the relation (Schoenberg and Helbig, 1997)

$$c_{13}(c_{22} + c_{12}) = c_{23}(c_{11} + c_{12}). \quad (4)$$

The existence of the additional constraint (4) stems from the fact that while general orthorhombic media are characterized by nine independent values of c_{ij}, the fracture-induced model considered here is defined by only eight quantities (for a fixed fracture orientation): five stiffness coefficients (c_{11_b}, c_{13_b}, c_{33_b}, c_{44_b}, and c_{66_b}) of the VTI background and three fracture weaknesses (Δ_N, Δ_V, and Δ_H).

The inversion of surface data for the physical parameters of the fractures requires relating seismic signatures to the fracture weaknesses. The results of Grechka and Tsvankin (1999) and Grechka et al. (1999) show that, in orthorhombic media, such commonly used signatures as NMO velocities and AVO gradients are most concisely expressed through the dimensionless anisotropic coefficients introduced by Tsvankin (1997b). The definitions of Tsvankin's parameters $\epsilon^{(1,2)}$, $\delta^{(1,2,3)}$, and $\gamma^{(1,2)}$ in

terms of the stiffness elements c_{ij} are given in Appendix B. Substituting equations (1)–(3) for the stiffnesses of the fracture-induced orthorhombic model into equations (B-1)–(B-9) yields the anisotropic coefficients ϵ, δ, and γ as functions of Δ_N, Δ_V, and Δ_H.

Weak-anisotropy approximation

The exact expressions for Tsvankin's anisotropic parameters in terms of the weaknesses, however, are too complicated to give insight into the influence of the fractures on the effective anisotropic model. Therefore, we assume that Thomsen's (1986) coefficients ϵ_b, δ_b, and γ_b of the VTI background, along with the weaknesses Δ_N, Δ_V, and Δ_H, are small quantities of the same order. Linearization of the effective stiffness matrix in these small quantitites [equation (A-17)] shows that for weak anisotropy the effective anisotropic coefficients $\epsilon^{(1,2)}$, $\delta^{(1,2,3)}$, and $\gamma^{(1,2)}$ should represent the *sums* of the VTI background parameters ϵ_b, δ_b, and γ_b and the corresponding anisotropic coefficients of the HTI medium resulting from the fractures in an imaginary isotropic host rock sufficiently close to the VTI background model. This isotropic medium can be characterized, for instance, by the P- and S-wave velocities V_P and V_S equal to the vertical velocities V_{P0_b} and V_{S0_b} in the VTI background.

Since this result provides a theoretical basis for most of the subsequent discussion, we prove it for one of the anisotropic coefficients—the parameter $\epsilon^{(2)}$ defined by equation (B-3). Substituting the stiffnesses from equations (1) and (2) into equation (B-3) yields

$$\epsilon^{(2)} = \frac{c_{11_b} - c_{33_b} - \Delta_N\left(c_{11_b} - \dfrac{c_{13_b}^2}{c_{11_b}}\right)}{2c_{33_b}\left(1 - \Delta_N \dfrac{c_{13_b}^2}{c_{11_b}c_{33_b}}\right)}. \tag{5}$$

Using the definition of the coefficient ϵ_b in the VTI background medium [$\epsilon_b \equiv (c_{11_b} - c_{33_b})/(2c_{33_b})$; see Thomsen (1986)], equation (5) can be rewritten as

$$\epsilon^{(2)} = \frac{\epsilon_b - \Delta_N \dfrac{c_{11_b}^2 - c_{13_b}^2}{2c_{11_b}c_{33_b}}}{1 - \Delta_N \dfrac{c_{13_b}^2}{c_{11_b}c_{33_b}}}. \tag{6}$$

Linearizing this equation with respect to ϵ_b and Δ_N, we drop the anisotropic term in the denominator to obtain

$$\epsilon^{(2)} \approx \epsilon_b - \Delta_N \frac{c_{11_b}^2 - c_{13_b}^2}{2c_{11_b}c_{33_b}}. \tag{7}$$

Since $(c_{11_b}^2 - c_{13_b}^2)/(c_{11_b}c_{33_b})$ is multiplied by the already small weakness Δ_N, it can be replaced in the weak anisotropy approximation by the corresponding isotropic quantity $4g(1-g)$, where $g \equiv V_{S0_b}^2/V_{P0_b}^2$ is the ratio of the squared vertical S- and P-wave velocities in the background. Thus, equation (7) can be represented as

$$\epsilon^{(2)} \approx \epsilon_b - 2g(1-g)\Delta_N. \tag{8}$$

The combination $-2g(1-g)\Delta_N$ can be recognized as the linearization of the anisotropic coefficient $\epsilon^{(V)}$ (Rüger, 1997; Tsvankin, 1997a) in an HTI medium due to a single set of vertical fractures perpendicular to the x_1-axis that are embedded in a purely isotropic rock with the squared S-to-P velocity ratio g (part I). Hence, equation (8) implies that

$$\epsilon^{(2)} \approx \epsilon_b + \epsilon^{(V)}. \tag{9}$$

We conclude that in the weak anisotropy limit the anisotropic coefficient $\epsilon^{(2)}$ reduces to the sum of the Thomsen background parameter ϵ_b and the coefficient $\epsilon^{(V)}$ of the HTI model due to the fractures embedded in an isotropic medium close enough to the VTI background medium. Similar linearizations for the other anisotropic parameters of the effective orthorhombic model are given below.

Symmetry plane [x_2, x_3] parallel to the fractures.—The linearized anisotropic coefficients in the symmetry plane [x_2, x_3], derived from equations (B-6)–(B-8), have the following form:

$$\epsilon^{(1)} = \epsilon_b, \tag{10}$$

$$\delta^{(1)} = \delta_b, \tag{11}$$

and

$$\gamma^{(1)} = \gamma_b + \frac{\Delta_V - \Delta_H}{2}. \tag{12}$$

Therefore, for weak anisotropy coefficients $\epsilon^{(1)}$ and $\delta^{(1)}$ coincide with those of the VTI background medium. This is an expected result; if rotationally invariant fractures are introduced into an isotropic matrix, the plane [x_2, x_3] represents the so-called isotropy plane of the effective HTI medium. In the isotropy plane the velocities of all waves are not influenced by the fractures and remain constant for all propagation directions (e.g., Tsvankin, 1997a). The coefficient $\gamma^{(1)}$ does not coincide with γ_b only because, in contrast to the more conventional model from part I, the fractures considered here are not rotationally invariant (i.e., $\Delta_V \neq \Delta_H$). The difference between Δ_V and Δ_H, however, has no bearing on parameters $\epsilon^{(1)}$ and $\delta^{(1)}$.

In addition to the basic set of anisotropic parameters introduced by Tsvankin (1997b), it is useful to consider the anellipticity coefficients $\eta^{(1,2,3)}$ responsible for time processing of P-wave data (Grechka and Tsvankin, 1999). For weak anisotropy, the η coefficient in the [x_2, x_3]-plane given by equation (B-10) is also equal to the background value:

$$\eta^{(1)} = \eta_b. \tag{13}$$

Symmetry plane [x_1, x_3] perpendicular to fractures.—The weak-anisotropy approximations of the anisotropic coefficients in the plane [x_1, x_3] are given by

$$\epsilon^{(2)} = \epsilon_b - 2g(1-g)\Delta_N, \tag{14}$$

$$\delta^{(2)} = \delta_b - 2g[(1-2g)\Delta_N + \Delta_V], \tag{15}$$

$$\gamma^{(2)} = \gamma_b - \frac{\Delta_H}{2}, \tag{16}$$

and

$$\eta^{(2)} = \eta_b + 2g[\Delta_V - g\Delta_N]. \tag{17}$$

Each of the expressions (14)–(17) contains two terms with a distinctly different physical meaning. The first term is the corresponding anisotropic coefficient of the VTI background,

while the second term absorbs the influence of the fractures. As discussed above for $\epsilon^{(2)}$, the fracture-related terms in equations (14)–(17) are approximately equal (assuming $\Delta_H = \Delta_V$) to the coefficients $\epsilon^{(V)}, \delta^{(V)}, \gamma^{(V)}$, and $\eta^{(V)}$ (respectively) derived in part I for a fracture set embedded in an isotropic background.

The constraint on the effective stiffnesses [equation (4)] leads to an additional relationship between the anisotropic coefficients. In the weak anisotropy limit, equation (4) can be rewritten as

$$\gamma^{(2)} - \gamma^{(1)} = \frac{1}{4g}\left[\delta^{(2)} - \delta^{(1)} - \left(\epsilon^{(2)} - \epsilon^{(1)}\right)\frac{1-2g}{1-g}\right]. \quad (18)$$

It is interesting that the background parameters and the tangential compliance Δ_H have no influence on constraint (18), which depends only on the differences between the anisotropic coefficients in the vertical symmetry planes, i.e., on $\epsilon^{(V)}$, $\delta^{(V)}$, and $\gamma^{(V)}$. As a result, equation (18) is analogous to the constraint given by Tsvankin (1997a) and part I for HTI media due to rotationally invariant fractures (i.e., for $\Delta_H = \Delta_V$).

Horizontal symmetry plane [x_1, x_2].—The only Tsvankin's (1997b) anisotropic coefficient defined in the horizontal plane is $\delta^{(3)}$ [equation (B-9)]. After linearization, it becomes

$$\delta^{(3)} = 2g[\Delta_N - \Delta_H]. \quad (19)$$

The parameter $\delta^{(3)}$ does not contain any background anisotropic coefficients because $[x_1, x_2]$ is the isotropy plane of the VTI medium. Since $\delta^{(3)}$ is defined with respect to the x_1-axis, which is normal to the fractures, equation (19) coincides with the expression for the generic Thomsen coefficient δ obtained for VTI media due to horizontal fractures by Schoenberg and Douma (1988).

The linearized anellipticity coefficient $\eta^{(3)}$ [equation (B-12)] has the form

$$\eta^{(3)} = 2g[\Delta_H - g\Delta_N]. \quad (20)$$

Estimation of the anisotropic parameters from reflection data

Inversion of reflection data for the effective parameters of orthorhombic media is discussed by Grechka and Tsvankin (1998, 1999), Rüger (1998), and Grechka et al. (1999). We now give a brief overview of their parameter-estimation methods operating with either wide-azimuth P-wave data or a combination of azimuthally dependent signatures of P- and PS-waves.

***P*-wave signatures.**—NMO velocity of P-waves in a horizontal orthorhombic layer is described by an ellipse with the axes in the vertical symmetry planes (Grechka and Tsvankin, 1998). Since for both orthorhombic models considered here the orientation of the symmetry planes is determined by the strike of the fractures, the axes of the P-wave NMO ellipse yield the fracture azimuth(s). In the orthorhombic model due to a single fracture set, $\delta^{(1)} > \delta^{(2)}$ [see equation (32)] and the semimajor axis of the P-wave NMO ellipse points in the direction of the fracture plane. This result holds for horizontal transverse isotropy as well (part I).

If $\delta^{(1)} = \delta^{(2)}$ and the P-wave NMO velocity from a horizontal reflector is azimuthally independent (i.e., the ellipse degenerates into a circle), the azimuths of the symmetry planes can be obtained from the NMO ellipse of a dipping event (Grechka and Tsvankin, 1999). P-wave reflection traveltimes from dipping interfaces or the azimuthal variation of nonhyperbolic moveout (Al-Dajani et al., 1998) can also be inverted for the anellipticity coefficients $\eta^{(1)}$, $\eta^{(2)}$, and $\eta^{(3)}$ [equations (13), (17), and (20)]. Nonnegligible values of both $\eta^{(1)}$ and $\eta^{(2)}$ help to detect the presence of anisotropy in the background and discriminate between HTI and orthorhombic models. For HTI media, all anisotropic coefficients (including η) in one of the symmetry planes should go to zero.

The semiaxes $V^{(1)}_{P,\mathrm{nmo}}$ and $V^{(2)}_{P,\mathrm{nmo}}$ of the P-wave NMO ellipse from a horizontal reflector are given by (Grechka and Tsvankin, 1998)

$$V^{(i)}_{P,\mathrm{nmo}} = V_{P0}\sqrt{1+2\delta^{(i)}}, \quad (i = 1, 2). \quad (21)$$

Hence, $V^{(i)}_{P,\mathrm{nmo}}$ can be combined with the vertical velocity V_{P0} to determine $\delta^{(1)}$ and $\delta^{(2)}$. If V_{P0} is unknown, the P-wave NMO ellipse constrains the difference χ between the two δ coefficients:

$$\chi \equiv \frac{\left(V^{(2)}_{P,\mathrm{nmo}}\right)^2 - \left(V^{(1)}_{P,\mathrm{nmo}}\right)^2}{\left(V^{(2)}_{P,\mathrm{nmo}}\right)^2 + \left(V^{(1)}_{P,\mathrm{nmo}}\right)^2} = \frac{\delta^{(2)} - \delta^{(1)}}{1 + \delta^{(2)} + \delta^{(1)}} \approx \delta^{(2)} - \delta^{(1)}. \quad (22)$$

Additional information for parameter estimation is provided by prestack amplitudes of P-waves. In the weak-anisotropy approximation, the variation of the P-wave amplitude variation with offset (AVO) gradient between the vertical symmetry planes is governed by the expression $\delta^{(2)} - \delta^{(1)} - 8g(\gamma^{(2)} - \gamma^{(1)})$ (Rüger, 1998). Therefore, if the squared velocity ratio g is known and $\delta^{(2)} - \delta^{(1)}$ has been found from the P-wave NMO ellipse [equation (22)], the AVO gradient yields an estimate of $\gamma^{(2)} - \gamma^{(1)}$.

***P*- and *PS*-wave signatures.**—Although P-wave data alone may be used to estimate a subset of the effective parameters of orthorhombic media, it is highly beneficial to combine P-wave traveltimes or amplitudes with the signatures of shear or converted waves. Since S-waves are not generated in most exploration surveys, we emphasize the joint inversion of P-waves and P- to S-mode conversions. The vertical traveltimes of P- and PS-waves give a direct estimate of the vertical-velocity ratio needed to compute the fracture weaknesses. The shear-wave splitting parameter at vertical incidence, conventionally evaluated from the time delays between the fast and slow shear or converted waves, is close to $\gamma^{(2)} - \gamma^{(1)}$. Also, the difference between the AVO gradients of the PS-wave in the vertical symmetry planes can be combined with the azimuthal variation of the P-wave AVO gradient or the P-wave NMO ellipse to obtain another estimate of $\gamma^{(2)} - \gamma^{(1)}$. A more detailed discussion of the azimuthal AVO inversion of PS-waves is given in part I.

Grechka et al. (1999) outline the following methodology of the joint moveout inversion of P- and PS-waves. Similar to pure modes, the azimuthally varying NMO velocity of either split PS-wave in a horizontal orthorhombic layer is described by an ellipse aligned with the vertical symmetry planes. The semiaxes of the NMO ellipses of the P- and two split PS-waves (i.e., the symmetry-plane NMO velocities) can be used to reconstruct the NMO ellipses of the pure shear waves S_1 and S_2. Assuming that wave S_1 represents an SV (in-plane polarized) mode in the $[x_2, x_3]$-plane [the superscript (1)], the semiaxes of

the shear-wave ellipses are expressed as

$$V^{(2)}_{S1,\,\mathrm{nmo}} = V_{S1}\sqrt{1+2\gamma^{(2)}} = V^{(1)}_{S2,\,\mathrm{nmo}}, \tag{23}$$

$$V^{(1)}_{S1,\,\mathrm{nmo}} = V_{S1}\sqrt{1+2\sigma^{(1)}}, \tag{24}$$

$$V^{(2)}_{S2,\,\mathrm{nmo}} = V_{S2}\sqrt{1+2\sigma^{(2)}}, \tag{25}$$

and

$$V^{(1)}_{S2,\,\mathrm{nmo}} = V_{S2}\sqrt{1+2\gamma^{(1)}} = V^{(2)}_{S1,\,\mathrm{nmo}}. \tag{26}$$

Here $\sigma^{(1)}$ and $\sigma^{(2)}$ are the anisotropic coefficients

$$\sigma^{(1)} \equiv \left(\frac{V_{P0}}{V_{S1}}\right)^2\left(\epsilon^{(1)} - \delta^{(1)}\right) \tag{27}$$

and

$$\sigma^{(2)} \equiv \left(\frac{V_{P0}}{V_{S2}}\right)^2\left(\epsilon^{(2)} - \delta^{(2)}\right), \tag{28}$$

and V_{S1} and V_{S2} are the vertical velocities of the split shear waves S_1 and S_2:

$$V_{S1} = V_{S2}\sqrt{\frac{1+2\gamma^{(1)}}{1+2\gamma^{(2)}}} \tag{29}$$

and

$$V_{S2} = V_{S0}. \tag{30}$$

If one of the vertical velocities or the reflector depth is known and the anisotropic parameters $\delta^{(1,2)}$ have been obtained from P-wave moveout, the shear-wave NMO ellipses make it possible to find four additional coefficients—$\epsilon^{(1,2)}$ and $\gamma^{(1,2)}$. The only anisotropic parameter not constrained by conventional-spread normal moveout in a horizontal orthorhombic layer is $\delta^{(3)}$.

Estimation of fracture parameters

Inversion for the weaknesses.—Since we are mostly interested in evaluating the properties of the fracture set, it is convenient to remove the influence of the background medium at the outset of the inversion procedure. Inspection of equations (10)–(17) shows that the contribution of the VTI background parameters can be eliminated by computing the *difference* between the anisotropic coefficients in the planes parallel and orthogonal to the fractures:

$$\epsilon^{(2)} - \epsilon^{(1)} = -2g(1-g)\Delta_N, \tag{31}$$

$$\delta^{(2)} - \delta^{(1)} = -2g[(1-2g)\Delta_N + \Delta_V] \approx \chi, \tag{32}$$

$$\gamma^{(2)} - \gamma^{(1)} = -\frac{\Delta_V}{2}, \tag{33}$$

$$\eta^{(2)} - \eta^{(1)} = 2g[\Delta_V - g\Delta_N]. \tag{34}$$

Equations (31)–(34) are identical to the expressions for $\epsilon^{(V)}$, $\delta^{(V)}$, $\gamma^{(V)}$, and $\eta^{(V)}$ (respectively) in HTI media due to a single set of vertical rotationally invariant fractures with the weaknesses Δ_N and Δ_V (part I). Therefore, the weaknesses can be determined from equations (31)–(34) using the HTI expressions described in detail in part I. We emphasize that obtaining Δ_N and Δ_V requires knowledge of any two of the differences $\epsilon^{(2)} - \epsilon^{(1)}$, $\delta^{(2)} - \delta^{(1)}$, $\gamma^{(2)} - \gamma^{(1)}$, and $\eta^{(2)} - \eta^{(1)}$.

As discussed, $\chi \approx \delta^{(2)} - \delta^{(1)}$ can be estimated from the elongation of the P-wave NMO ellipse for horizontal events [equation (22)]. Also, $\eta^{(2)}$ and $\eta^{(1)}$ can be obtained using the NMO velocities of dipping P-events or nonhyperbolic moveout. Thus, P-wave moveout data provide sufficient information to determine the weaknesses Δ_N and Δ_V from equations (32) and (34):

$$\Delta_N = -\frac{\left(\delta^{(2)} - \delta^{(1)}\right) + \left(\eta^{(2)} - \eta^{(1)}\right)}{2g(1-g)}, \tag{35}$$

$$\Delta_V = \frac{1}{2(1-g)}\left[\frac{1-2g}{g}\left(\eta^{(2)} - \eta^{(1)}\right) - \left(\delta^{(2)} - \delta^{(1)}\right)\right]. \tag{36}$$

In principle, the inversion based on equations (35) and (36) requires knowledge of the squared vertical-velocity ratio g, which cannot be found without shear or converted-wave data. However, numerical tests (and the results of part I) show that even a relatively rough estimate of g is sufficient for recovering the weaknesses with acceptable accuracy.

P-wave moveout data may provide not just the difference between $\eta^{(2)}$ and $\eta^{(1)}$ but also the individual values of these coefficients. Therefore, in addition to substituting $\eta^{(2)} - \eta^{(1)}$ into the equations for the weaknesses, we can use the approximate relation (13), $\eta^{(1)} = \eta_b$, to determine the η coefficient in the background VTI model.

If the P-wave moveout information is limited to the NMO ellipse from a horizontal reflector, it is possible to obtain the difference $\gamma^{(2)} - \gamma^{(1)}$ by including the P-wave AVO gradients in the directions parallel and perpendicular to the fractures. The algorithm based on the NMO ellipses of horizontal events and AVO gradients is identical to the one described in part I for HTI media. The presence of anisotropy in the background has no influence either on estimating $\delta^{(2)} - \delta^{(1)}$ and $\gamma^{(2)} - \gamma^{(1)}$ or on inverting these differences [equations (32) and (33)] for the weaknesses Δ_N and Δ_V.

In multicomponent surveys, the vertical traveltimes of PS-waves (in combination with P-wave data) provide estimates of g and the splitting coefficient $\gamma^{(2)} - \gamma^{(1)}$. Thus, another possible set of input parameters includes the P-wave NMO ellipse from a horizontal reflector (yielding $\delta^{(2)} - \delta^{(1)}$) and the vertical traveltimes of converted modes.

Note that the weakness Δ_H does not enter any of the differences (31)–(34), despite the fact that it appears in equations (12) and (16) for $\gamma^{(1)}$ and $\gamma^{(2)}$. However, even the individual values of $\gamma^{(1)}$ and $\gamma^{(2)}$ constrain the combination $\gamma_b - \Delta_H/2$ but not Δ_H separately. The only source of information about Δ_H is $\eta^{(3)}$ or $\delta^{(3)}$ [equations (19) and (20)], which can be estimated using the NMO velocities of P-wave reflections from dipping interfaces (Grechka and Tsvankin, 1999):

$$\Delta_H = \frac{\eta^{(3)}}{2g} + g\Delta_N. \tag{37}$$

If dipping events are not available, the data cannot be inverted for the coefficient $\eta^{(3)}$ and, therefore, for the weakness Δ_H. In this case, a reasonable simplifying assumption is that the fractures are rotationally invariant and $\Delta_V = \Delta_H$. Then the number of independent medium parameters reduces to seven, and $\delta^{(3)}$ and $\eta^{(3)}$ can be expressed as

$$\delta^{(3)} = \delta^{(2)} - \delta^{(1)} - 2\left(\epsilon^{(2)} - \epsilon^{(1)}\right), \tag{38}$$

$$\eta^{(3)} = \eta^{(2)} - \eta^{(1)}. \tag{39}$$

Interpretation of the weaknesses in terms of the physical properties of the fractures is discussed in part I. For rotationally invariant penny-shaped cracks, the tangential weakness $\Delta_V = \Delta_H$ gives an estimate of the crack density, while the normal weakness Δ_N represents a sensitive, albeit nonunique, indicator of fluid content.

Numerical examples.—Although the weak-anisotropy approximations provide useful insight into the parameter estimation problem, it is preferable to use the exact equations for actual inversion. In the examples below, we compute the fracture weaknesses Δ_N, Δ_V, and Δ_H, along with the anisotropic coefficient η_b of the background, by inverting the values of χ [equation (22)], $\eta^{(1)}$, $\eta^{(2)}$, and $\eta^{(3)}$ presumably extracted from P-wave seismic data. The goal of this numerical study is to examine the sensitivity of the inverted parameters to errors in the input data and in the parameters of the background medium.

Our nonlinear inversion algorithm is based on equations (1)–(3) for the stiffness elements and on the exact expressions for the anisotropic coefficients given in Appendix B. The weak-anisotropy approximations (13) and (35)–(37) are used only to obtain the initial guesses for the weaknesses and the coefficient η_b. The parameters of the background medium are $g = V_{S0b}^2/V_{P0b}^2 = 0.25, \delta_b = 0.2$, and $\gamma_b = 0.1$ (ϵ_b can be expressed through δ_b and η_b). Although the only background parameter in equations (35)–(37) is the squared velocity ratio g, the anisotropic coefficients δ_b and γ_b of the VTI medium are contained in the exact equations for the stiffnesses and effective anisotropic parameters and must be specified for the inversion. As shown below, however, the inversion results are insensitive to variations of g, δ_b, and γ_b within the range important in practice. The fracture set is defined by the weaknesses $\Delta_N = 0.5$ and $\Delta_V = \Delta_H = 0.2$, which approximately correspond to values for penny-shaped gas-filled cracks (see part I).

The inversion results are displayed in Figure 1. For the correct input parameters (and the correct background parameters g, δ_b, and γ_b), the inversion algorithm produces accurate values of the weaknesses and η_b. Errors in the measured anisotropic parameters of up to ± 0.1 result in similar (often smaller) errors in the inverted values, indicating that the parameter estimation procedure is reasonably stable. As expected from the analytic results, different inverted parameters are most sensitive to errors in different measured quantities. For example, errors in χ produce comparable distortions in all three weaknesses, reaching and sometimes exceeding ± 0.1 (Figure 1a). The anellipticity coefficient η_b is quite sensitive to errors in $\eta^{(1)}$ (Figure 1b) and is almost independent of the other input parameters, in accordance with the weak-anisotropy approximation (13). Errors in $\eta^{(1)}$ and $\eta^{(2)}$ of about ± 0.1 cause smaller errors (± 0.05) in the tangential weaknesses Δ_V and Δ_H than in the normal weakness Δ_N (± 0.1; Figures 1b,c). The weakness Δ_H is sensitive primarily to errors in $\eta^{(3)}$ (Figure 1d), as suggested by equation (37). In the weak-anisotropy limit, Δ_N and Δ_V are independent of $\eta^{(3)}$ [equations (35) and (36)], which is confirmed by Figure 1d.

In the second test, we examine the influence of errors in the background parameters g, δ_b, and γ_b (which were assumed known a priori in the previous example) on the inversion

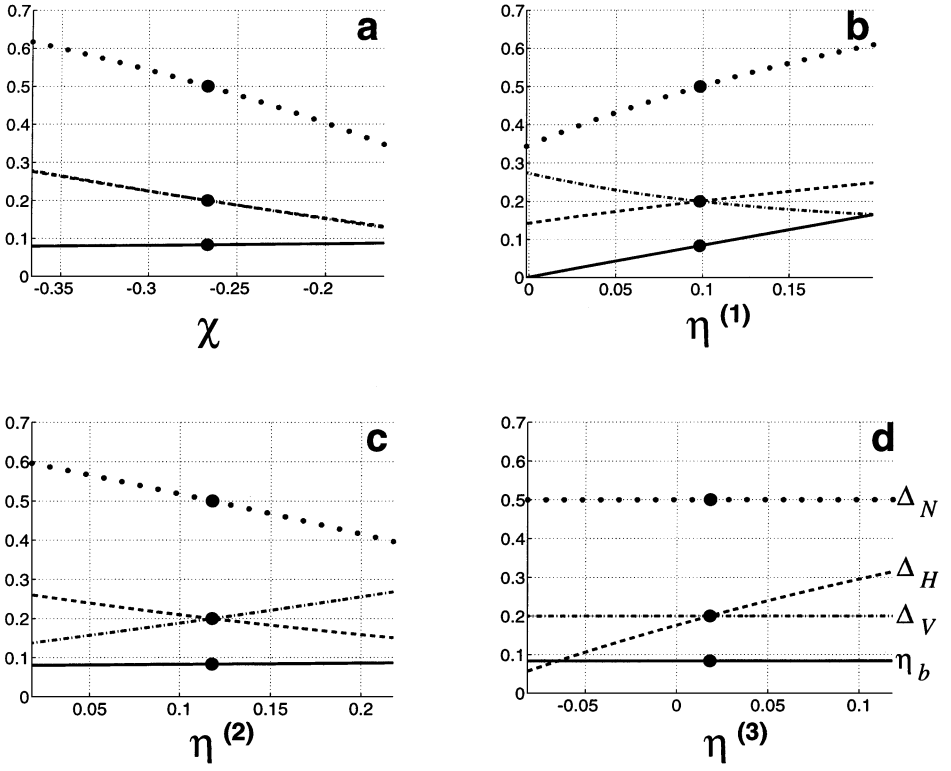

FIG. 1. Numerical inversion of χ, $\eta^{(1)}$, $\eta^{(2)}$, and $\eta^{(3)}$ for the fracture weaknesses Δ_N (dotted line), Δ_V (dash-dotted), Δ_H (dashed), and the coefficient η_b of the background medium (solid). Errors of ± 0.1 were introduced in (a) χ, (b) $\eta^{(1)}$, (c) $\eta^{(2)}$, and (d) $\eta^{(3)}$, with the other input parameters held at the correct values. In the absence of errors, the inversion yields the correct values of the weaknesses and η_b (large dots).

results. Substantial errors in g of ± 0.1, or up to 40%, lead to relatively small distortions of only about ± 0.03 in all inverted parameters except Δ_N (for Δ_N the errors reach ± 0.1; Figure 2a). The anisotropic coefficients δ_b and γ_b have an even smaller influence on the estimated quantities, especially on the tangential compliances (Figure 2b,c). This result is especially encouraging because δ_b and γ_b are difficult to estimate from surface seismic data without information about the vertical velocities or reflector depth.

Estimation of background parameters.—As discussed above, the individual values of the anisotropic parameters $\epsilon^{(1,2)}$, $\delta^{(1,2)}$, and $\gamma^{(1,2)}$ can be found by combining P-wave moveout data with the reflection traveltimes of PS-waves (provided the reflector depth is known). Then it is possible to estimate not just the fracture weaknesses but also the squared vertical-velocity ratio g and the background anisotropic parameters ϵ_b, δ_b, and γ_b [equations (10)–(12); to find γ_b, we assume $\Delta_V = \Delta_H$].

For the numerical example in Figure 3, the input data included the vertical and NMO velocities of P- and split S-waves, where the shear-wave signatures were supposedly determined from P and PS data. The NMO velocity of each mode was computed in three azimuthal directions with a step of 45° and approximated with an ellipse to find the NMO velocities in the symmetry planes. Then the vertical velocities and symmetry-plane NMO velocities were combined to determine $\epsilon^{(1,2)}$, $\delta^{(1,2)}$, and $\gamma^{(1,2)}$ from equations (21) and (23)–(26). To check the influence of measurement errors, we added Gaussian noise with a standard deviation of 2% to the vertical and NMO velocities and performed the inversion for 200 sets of the distorted input parameters. The algorithm is based on the exact expressions for the anisotropic coefficients derived from equations (1)–(3), with the starting model computed using the weak-anisotropy approximation. Since the inversion errors in Figure 3 are limited by ± 0.05, the estimation of both weaknesses and all background parameters is sufficiently stable.

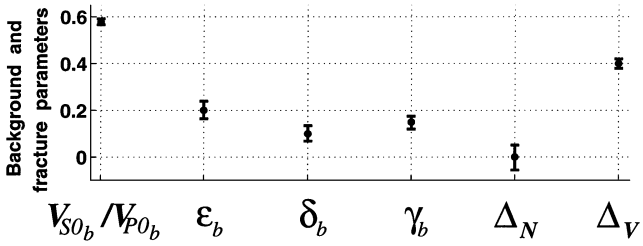

FIG. 3. Inversion of the vertical and NMO velocities of the P- and split S-waves for the parameters of the fractures and VTI background. The dots mark the correct values of the parameters; it is assumed that $\Delta_V = \Delta_H$. The bars correspond to $\pm$ one standard deviation in the inverted quantities caused by Gaussian noise in the input data with a standard deviation of 2%.

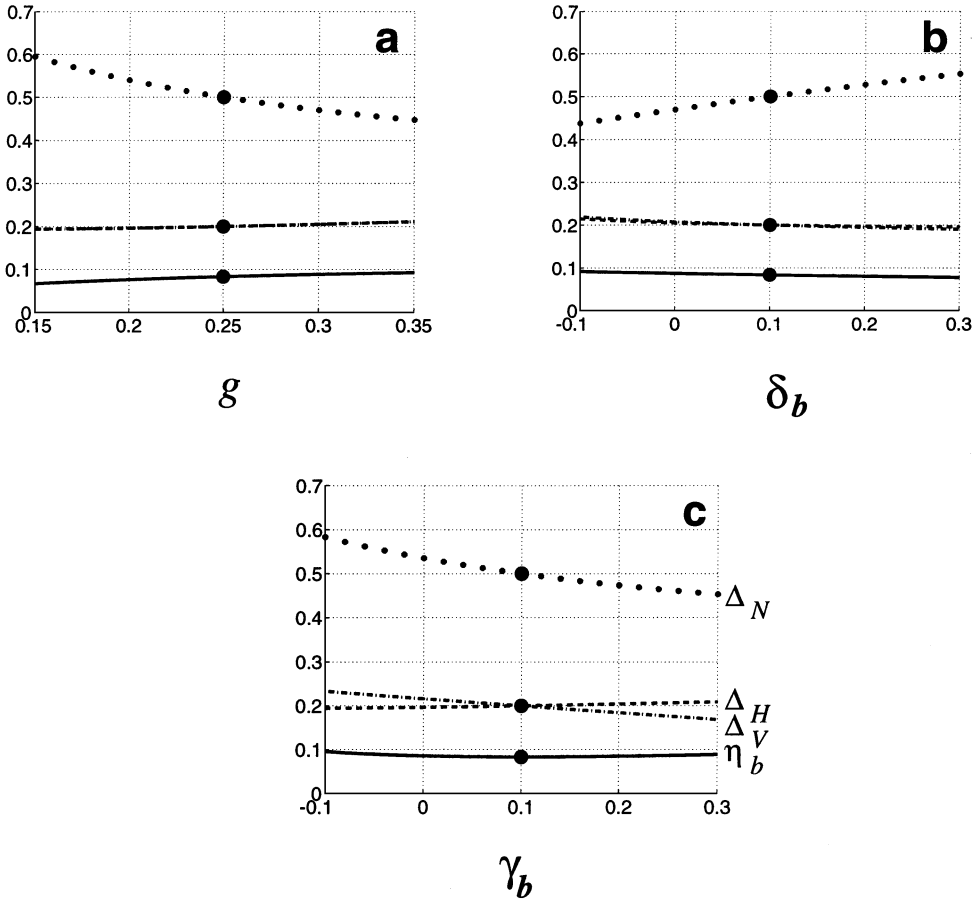

FIG. 2. Influence of the background parameters (a) $g = V_{S0_b}^2/V_{P0_b}^2$, (b) δ_b, and (c) γ_b on the inversion results from Figure 1 for the correct values of χ and $\eta^{(1,2,3)}$. Dotted line—Δ_N; dash-dotted—Δ_V; dashed—Δ_H; solid—η_b.

MODEL 2: TWO ORTHOGONAL FRACTURE SETS IN ISOTROPIC ROCK

Another practically important fractured model with orthorhombic symmetry is composed of two orthogonal vertical fracture sets embedded in an isotropic or VTI background. To simplify the parameter estimation procedure, we assume that the fractures are rotationally invariant and the background matrix is purely isotropic. Choosing the x_1-axis to be perpendicular to the first set of fractures, we obtain the compliance matrices for both fracture systems in equations (A-3) and (A-14) where, because of the rotational invariance, the compliances satisfy $K_{V1} = K_{H1} \equiv K_{T1}$ and $K_{V2} = K_{H2} \equiv K_{T2}$. Building the effective matrix of the excess compliance [equation (A-12)] and adding the compliance of the isotropic background yields the effective stiffness matrix [equation (A-1)]

$$\mathbf{c} = \begin{pmatrix} c_{11} & c_{12} & c_{13} & 0 & 0 & 0 \\ c_{12} & c_{22} & c_{23} & 0 & 0 & 0 \\ c_{13} & c_{23} & c_{33} & 0 & 0 & 0 \\ 0 & 0 & 0 & c_{44} & 0 & 0 \\ 0 & 0 & 0 & 0 & c_{55} & 0 \\ 0 & 0 & 0 & 0 & 0 & c_{66} \end{pmatrix} = \left(\begin{array}{c|c} \tilde{\tilde{\mathbf{c}}}_1 & \mathbf{0} \\ \hline \mathbf{0} & \tilde{\tilde{\mathbf{c}}}_2 \end{array}\right), \tag{40}$$

where $\mathbf{0}$ is the 3×3 zero matrix and the matrices $\tilde{\tilde{\mathbf{c}}}_1$ and $\tilde{\tilde{\mathbf{c}}}_2$ are given by

$$\tilde{\tilde{\mathbf{c}}}_1 = \frac{1}{d} \begin{pmatrix} (\lambda+2\mu) l_1 m_3 & \lambda l_1 m_1 & \lambda l_1 m_2 \\ \lambda l_1 m_1 & (\lambda+2\mu) l_3 m_1 & \lambda l_2 m_1 \\ \lambda l_1 m_2 & \lambda l_2 m_1 & (\lambda+2\mu)(l_3 m_3 - l_4) \end{pmatrix}, \tag{41}$$

$$\tilde{\tilde{\mathbf{c}}}_2 = \begin{pmatrix} \mu(1-\Delta_{T2}) & 0 & 0 \\ 0 & \mu(1-\Delta_{T1}) & 0 \\ 0 & 0 & \mu\dfrac{(1-\Delta_{T1})(1-\Delta_{T2})}{(1-\Delta_{T1}\Delta_{T2})} \end{pmatrix}. \tag{42}$$

Here, λ and μ are the Lamé parameters of the background medium and

$$\begin{gathered} l_1 = 1-\Delta_{N1}, \quad l_2 = 1 - r\Delta_{N1}, \quad l_3 = 1 - r^2\Delta_{N1}, \\ l_4 = 4r^2 g^2 \Delta_{N1}\Delta_{N2}, \\ m_1 = 1-\Delta_{N2}, \quad m_2 = 1 - r\Delta_{N2}, \quad m_3 = 1 - r^2\Delta_{N2}, \\ g = \mu/(\lambda+2\mu) = V_S^2/V_P^2, \quad r = 1-2g, \\ d = 1 - r^2\Delta_{N1}\Delta_{N2}. \end{gathered} \tag{43}$$

The values Δ_{Ni} and Δ_{Ti} $(i = 1, 2)$ are the normal and tangential fracture weaknesses (see part I) related to the fracture compliances by the equations

$$\Delta_{Ni} = \frac{K_{Ni}(\lambda+2\mu)}{1 + K_{Ni}(\lambda+2\mu)} \tag{44}$$

and

$$\Delta_{Ti} = \frac{K_{Ti}\mu}{1 + K_{Ti}\mu}, \tag{45}$$

which represent a special case (valid for an isotropic background) of equations (A-4).

Since both fracture planes and the horizontal plane constitute three orthogonal planes of mirror symmetry, the effective medium must be orthorhombic with the nine stiffness elements [equation (40)]. Our model, however, represents a special case of general orthorhombic media with only six independent parameters: λ, μ, Δ_{N1}, Δ_{T1}, Δ_{N2}, and Δ_{T2}. As follows from equations (41) and (42), the three additional relationships (constraints) between the stiffnesses are

$$c_{12}(c_{33} + c_{23}) = c_{13}(c_{22} + c_{23}), \tag{46}$$

$$2\,(c_{11} + c_{13}) = \left(c_{11}c_{33} - c_{13}^2\right)\left(\frac{c_{44}+c_{55}}{c_{44}c_{55}} - \frac{1}{c_{66}}\right), \tag{47}$$

and

$$2(c_{22} + c_{23}) = \left(c_{22}c_{33} - c_{23}^2\right)\left(\frac{c_{44}+c_{55}}{c_{44}c_{55}} - \frac{1}{c_{66}}\right). \tag{48}$$

Models with two identical orthogonal fracture sets, characterized by fewer independent parameters, are discussed in Appendix C.

Anisotropic coefficients in the weak-anisotropy limit

Equations (40)–(43), combined with the definitions from Appendix B, can be used to express Tsvankin's (1997b) anisotropic coefficients in terms of the fracture weaknesses Δ_{Ti} and Δ_{Ni}. Here we restrict ourselves to linearized expressions obtained in the limit of small fracture compliances $\Delta_{T1,2} \ll 1$ and $\Delta_{N1,2} \ll 1$. The result of this linearization can be predicted from equation (A-13): since in the linear approximation fracture systems are not influenced by each other, the effective orthorhombic medium is composed of two HTI media produced by each fracture set individually.

Symmetry plane $[x_2, x_3]$.—The anisotropic parameters with the superscript (1) are defined in the symmetry plane $[x_2, x_3]$, which is parallel to the first set of fractures and orthogonal to the second one. In the absence of the second set, the $[x_2, x_3]$-plane would coincide with the isotropy plane of the HTI medium associated with the first fracture system. Therefore, we can expect these parameters to be largely influenced by the second set of fractures orthogonal to the x_2-axis. Indeed, the linearized ϵ, δ, γ, and η coefficients in the $[x_2, x_3]$ plane depend only on the weaknesses Δ_{N2} and Δ_{T2}:

$$\epsilon^{(1)} = -2g(1-g)\Delta_{N2}, \tag{49}$$

$$\delta^{(1)} = -2g[(1-2g)\Delta_{N2} + \Delta_{T2}], \tag{50}$$

$$\gamma^{(1)} = -\frac{\Delta_{T2}}{2}, \tag{51}$$

$$\eta^{(1)} = 2g[\Delta_{T2} - g\Delta_{N2}], \tag{52}$$

where $g \equiv V_S^2/V_P^2$ is the ratio of the squared S- and P-wave velocities in the background. Equations (49)–(52) coincide with the expressions for the anisotropic coefficients $\epsilon^{(V)}$, $\delta^{(V)}$, $\gamma^{(V)}$, and $\eta^{(V)}$ of the HTI model associated with the second fracture set.

Symmetry plane $[x_1, x_3]$.—Likewise, the linearized anisotropic coefficients in the symmetry plane $[x_1, x_3]$ are governed by the weaknesses of the first fracture set. As follows from the symmetry of the model, the expressions for $\epsilon^{(2)}$, $\delta^{(2)}$, $\gamma^{(2)}$, and $\eta^{(2)}$ are fully analogous to equations (49)–(52):

$$\epsilon^{(2)} = -2g(1-g)\Delta_{N1}, \tag{53}$$

$$\delta^{(2)} = -2g[(1-2g)\Delta_{N1} + \Delta_{T1}], \tag{54}$$

$$\gamma^{(2)} = -\frac{\Delta_{T1}}{2}, \tag{55}$$

$$\eta^{(2)} = 2g[\Delta_{T1} - g\Delta_{N1}]. \tag{56}$$

Symmetry plane $[x_1, x_2]$.—The remaining anisotropic coefficient $\delta^{(3)}$ defined in the horizontal symmetry plane $[x_1, x_2]$ is given by

$$\delta^{(3)} = 2g[\Delta_{N1} - \Delta_{T1}] - 2g[(1-2g)\Delta_{N2} + \Delta_{T2}]. \tag{57}$$

The linearized parameter $\delta^{(3)}$ is equal to the sum of the generic Thomsen coefficient δ caused by horizontal fractures in VTI media (the term $2g[\Delta_{N1} - \Delta_{T1}]$; see Schoenberg and Douma, 1988) and the HTI coefficient $\delta^{(V)}$ is due to vertical fractures (part I). To explain this result, recall that $\delta^{(3)}$ is defined with respect to the x_1-axis, which is orthogonal to the first fracture set (so this set becomes horizontal if the x_1-axis is made vertical in VTI media) and lies in the planes of the second set of fractures (making this set vertical).

The anellipticity coefficient $\eta^{(3)}$ [equation (B-12] in the horizontal plane is

$$\eta^{(3)} = \eta^{(1)} + \eta^{(2)}. \tag{58}$$

Relations between anisotropic coefficients.—The nine stiffnesses of the effective orthorhombic model contain only six independent quantities, which leads to the three constraints (46)–(48). Rewriting equations (46) and (47) through Tsvankin's (1997b) parameters yields

$$\gamma^{(i)} = \frac{1}{4g}\left[\delta^{(i)} - \epsilon^{(i)}\frac{1-2g}{1-g}\right], \quad (i = 1, 2), \tag{59}$$

where quadratic and higher-order terms in the anisotropic coefficients were dropped. The same result can be obtained from the linearized expressions for the anisotropic coefficients given above. Equation (59) is identical to the relationship between $\epsilon^{(V)}$, $\delta^{(V)}$, and $\gamma^{(V)}$ of HTI media (Tsvankin, 1997a; part I).

The remaining constraint (48) takes the form

$$\delta^{(3)} = \delta^{(1)} + \delta^{(2)} - 2\epsilon^{(2)}. \tag{60}$$

Equations (59) and (60) show that in Tsvankin's notation our orthorhombic model can be fully described by the two vertical velocities and four anisotropic coefficients $\delta^{(1,2)}$ and $\epsilon^{(1,2)}$.

In the special case of penny-shaped gas-filled fractures, the normal and tangential compliances are equal to each other ($K_{N1} = K_{T1}$ and $K_{N2} = K_{T2}$) and, as noticed by Schoenberg and Sayers (1995), the anellipticity parameters in the symmetry planes go to zero:

$$\eta^{(1)} = \eta^{(2)} = \eta^{(3)} = 0. \tag{61}$$

Estimation of fracture parameters

The structure of equations (49)–(56) for the anisotropic coefficients suggests that estimation of the weaknesses of the orthogonal fracture sets can be decomposed into two HTI-type inversions in the vertical symmetry planes discussed in part I. Here, we verify the accuracy of the weak-anisotropy approximations and outline two possible strategies for obtaining the weaknesses from surface reflection data. One is based on azimuthally dependent P-wave reflection moveout alone; the other uses both P- and converted-wave data. In contrast to the model with a single fracture set, we must know one of the vertical velocities (or reflector depth) because the inversion algorithm requires the individual values of Tsvankin's anisotropic coefficients rather than their differences.

***P*-wave inversion.**—As for the model with a single fracture set, the fracture orientation can be determined directly from the P-wave NMO ellipse (or the NMO ellipses of converted waves), unless the ellipse degenerates into a circle. This and some other special cases are discussed in Appendix D. Suppose the parameters $\delta^{(1)}$ and $\delta^{(2)}$ have been found using the semiaxes of the P-wave NMO ellipse from a horizontal reflector and the vertical velocity [equations (21)]. Combining the δ coefficients with the anellipticity parameters $\eta^{(1)}$ and $\eta^{(2)}$ (also determined from P-wave moveout) allows us to solve equations (50), (52), (54), and (56) for the weaknesses

$$\Delta_{N1} = -\frac{\delta^{(2)} + \eta^{(2)}}{2g(1-g)}, \tag{62}$$

$$\Delta_{T1} = \frac{1}{2(1-g)}\left[\frac{1-2g}{g}\eta^{(2)} - \delta^{(2)}\right], \tag{63}$$

$$\Delta_{N2} = -\frac{\delta^{(1)} + \eta^{(1)}}{2g(1-g)}, \tag{64}$$

and

$$\Delta_{T2} = \frac{1}{2(1-g)}\left[\frac{1-2g}{g}\eta^{(1)} - \delta^{(1)}\right]. \tag{65}$$

The equations for each pair of weaknesses [(62)–(63) and (64)–(65)] are identical to those obtained in part I for HTI media due to a single set of rotationally invariant fractures.

To test the accuracy of the weak anisotropy approximations (62)–(65), we computed the exact anisotropic coefficients $\delta^{(1,2)}$ and $\eta^{(1,2)}$ for three fractured models in Table 1 [using equations (40)–(42) and the definitions from Appendix B] and inverted them for the weaknesses in the limit of weak anisotropy. Table 1 shows that approximations (62)–(65) give reasonably good estimates of the fracture weaknesses. The only significant error, in the tangential weakness of the second fracture set, is unrelated to the first set because it remains the same for the corresponding HTI model (third row in Table 1).

Inversion of *P*- and *PS*-wave data.—If dipping events are not available and CMP spreads are not sufficiently long for using nonhyperbolic moveout, it may be possible to find the anisotropic coefficients $\epsilon^{(1,2)}$, $\delta^{(1,2)}$, and $\gamma^{(1,2)}$ by combining P- and PS-wave data [equations (23)–(26)]. Since these anisotropic parameters depend on only four fracture weaknesses, P- and PS-wave data (including the vertical velocities or reflector depth) provide useful redundancy in the inversion procedure. In the weak-anisotropy approximation, the

weaknesses can be computed, for example, as

$$\Delta_{T1} = -2\gamma^{(2)} = 1 - \left(\frac{V^{(2)}_{S1,\mathrm{nmo}}}{V_{S1}}\right)^2, \tag{66}$$

$$\Delta_{T2} = -2\gamma^{(1)} = 1 - \left(\frac{V^{(1)}_{S2,\mathrm{nmo}}}{V_{S2}}\right)^2, \tag{67}$$

$$\Delta_{N1} = -\frac{1}{1-2g}\left[\Delta_{T1} + \frac{\delta^{(2)}}{2g}\right], \tag{68}$$

$$\Delta_{N2} = -\frac{1}{1-2g}\left[\Delta_{T2} + \frac{\delta^{(1)}}{2g}\right]. \tag{69}$$

Figure 4 shows the results of numerical inversion based on NMO equations (23)–(26) and the exact expressions for Tsvankin's anisotropic coefficients in terms of the fracture weaknesses. Similar to the numerical example in Figure 3, the vertical velocities and azimuthally varying NMO velocities of *P*- and *S*-waves (input data) were distorted by Gaussian noise with a standard deviation of 2%. The initial model was found from the weak-anisotropy approximations (66)–(69). The standard deviations for the inverted weaknesses are relatively small, with errors in the tangential compliances Δ_{T1} and Δ_{T2} being somewhat lower than those in Δ_{N1} and Δ_{N2}.

DISCUSSION AND CONCLUSIONS

Applying the linear-slip theory developed by Schoenberg (1980, 1983), we studied two types of orthorhombic media believed to be representative of naturally fractured reservoirs. The first model contains a single set of vertical fractures embedded in a VTI background (e.g., the background anisotropy may result from fine layering), while the second is produced by two orthogonal systems of rotationally invariant vertical fractures in an isotropic host rock. For both effective models we obtained Tsvankin's (1997b) anisotropic parameters, which capture the combinations of the stiffness coefficients responsible for commonly measured seismic signatures.

Table 1. Comparison of the actual fracture parameters with those estimated by inverting the exact anisotropic coefficients [equations (40)–(42) and Appendix B] using the linearized equations (62)–(65); the squared velocity ratio g = 0.25. The first model is composed of two orthogonal fracture sets in an isotropic background; the second and third models contain only one fracture set (i.e., they have the HTI symmetry).

Model	Fracture parameters	Δ_{N1}	Δ_{T1}	Δ_{N2}	Δ_{T2}
1	Actual	0.30	0.15	0.60	0.30
	Estimated	0.28	0.14	0.66	0.21
2	Actual	0.30	0.15	0	0
	Estimated	0.30	0.14	0	0
3	Actual	0	0	0.60	0.30
	Estimated	0	0	0.67	0.21

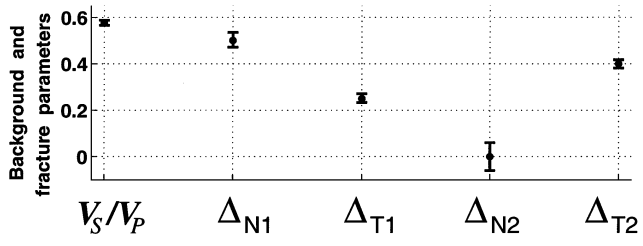

FIG. 4. Inversion of the *P*- and *S*-wave vertical and NMO velocities for the model with two orthogonal fracture sets. The input data were contaminated by Gaussian noise with a standard deviation of 2%, and the inversion was repeated 200 times for different realizations of the input parameters. The bars correspond to ± one standard deviation in the inverted quantities.

To gain a better understanding of the influence of fractures on the effective medium, we simplified the anisotropic parameters under the assumption of weak background and fracture-induced anisotropy. For the model with a single fracture set, the anisotropic parameters of the HTI medium due to the fractures are added to the background coefficients to produce the linearized effective parameters of the orthorhombic medium. Therefore, by computing the difference between the effective coefficients defined in the vertical symmetry planes, we eliminate the influence of the background and reduce the inverse problem to that for horizontal transverse isotropy (part I). The information necessary for this inversion procedure can be obtained from azimuthally dependent *P*-wave reflection traveltimes alone if dipping events or nonhyperbolic moveout are available (also, it is necessary to have an estimate of the ratio of the *P*- and *S*-wave vertical velocities). Alternatively, the inversion can be performed by combining the *P*-wave NMO ellipse from a horizontal reflector with other data, such as the azimuthally varying *P*-wave AVO gradient or the vertical traveltimes and, possibly, NMO velocities of the split converted (*PS*) modes. For weak anisotropy, the algorithm based on the NMO ellipses and AVO gradients of *P*- and *PS*-waves reflected from horizontal interfaces is identical to that outlined in part I for HTI media (i.e., it is independent of the presence of anisotropy in the background).

In the case of two orthogonal fracture sets, the linearized expressions for the effective anisotropic coefficients in each vertical symmetry plane contain only the contribution of the fractures orthogonal to this plane. As a result, the inversion for the fracture weaknesses splits into two separate inversion procedures in the symmetry planes, which can be carried out using the HTI algorithm of part I. In contrast to the model with a single fracture set, however, determination of the weaknesses of both fracture sets requires knowledge of the vertical velocities in addition to the azimuthally varying surface seismic signatures.

Although both effective media considered here have orthorhombic symmetry, the results of our analysis indicate several possible ways to identify the correct underlying physical model. In both cases, the stiffness tensor is described by fewer independent parameters than for general orthorhombic media, and the anisotropic coefficients for the models with one and two fracture sets satisfy different constraints. Another useful criterion is the sign of the anisotropic parameters. The coefficients $\epsilon^{(1,2)}$, $\delta^{(1,2)}$, and $\gamma^{(1,2)}$ for the model with two orthogonal systems of fractures in an isotropic background are negative [equations (49)–(51) and (53)–(55)]. In contrast, ϵ and γ (and often δ as well) defined in the fracture plane of the model with a single fracture set in a VTI background are usually positive. Also, we can distinguish between the two models by comparing the polarization direction of the vertically traveling fast shear wave with the orientation of the semimajor axis of the *P*-wave NMO ellipse. For one set of fractures (in either isotropic or VTI background), they always coincide with each other; for two systems of fractures with different fluid content, they may become orthogonal. This happens, for example, if the two

inequalities $\Delta_{T1} > \Delta_{T2}$ and $(1-2g)\Delta_{N1} + \Delta_{T1} < (1-2g)\Delta_{N2} + \Delta_{T2}$ (or, equivalently, $\delta^{(2)} > \delta^{(1)}$) are satisfied simultaneously.

ACKNOWLEDGMENTS

This research was carried out during a visit of Andrey Bakulin to the Center for Wave Phenomena (CWP), Colorado School of Mines, 1998. We are grateful to members of the A(nisotropy)-team of CWP for helpful discussions and to Andreas Rüger (Landmark) for his review of the manuscript. The support for this work was provided by the members of the Consortium Project on Seismic Inverse Methods for Complex Structures at CWP and by the U.S. Department of Energy (award #DE-FG03-98ER14908).

REFERENCES

Al-Dajani, A., Tsvankin, I., and Toksöz, N., 1998, Nonhyperbolic reflection moveout in azimuthally anisotropic media: 68th Ann. Internat. Mtg., Soc. Expl. Geophys., Expanded Abstracts, 1479–1482.

Alkhalifah, T., and Tsvankin, I., 1995, Velocity analysis in transversely isotropic media: Geophysics, **60**, 1550–1566.

Bakulin, A. V., and Molotkov, L. A., 1998, Effective models of fractured and porous media: St. Petersburg Univ. Press (in Russian).

Bakulin, A., Tsvankin, I., and Grechka, V., 2000, Estimation of fracture parameters from reflection seismic data–Part I: HTI model due to a single fracture set: Geophysics, **65**, 1788–1802, this issue.

Grechka, V., and Tsvankin, I., 1998, 3-D description of normal moveout in anisotropic inhomogeneous media: Geophysics, **63**, 1079–1092.

——— 1999, 3-D moveout velocity analysis and parameter estimation for orthorhombic media: Geophysics, **64**, 820–837.

Grechka, V., Theophanis, S., and Tsvankin, I., 1999, Joint inversion of *P*- and *PS*-waves in orthorhombic media: Theory and a physical-modeling study: Geophysics, **64**, 146–161.

Hudson, J. A., 1980, Overall properties of a cracked solid: Math. Proc. Camb. Phil. Soc., **88**, 371–384.

——— 1981, Wave speeds and attenuation of elastic waves in material containing cracks: Geophys. J. Roy. Astr. Soc., **64**, 133–150.

——— 1988, Seismic wave propagation through material containing partially saturated cracks: Geophys. J., **92**, 33–37.

Molotkov, L. A., and Bakulin, A. V., 1997, An effective model of a fractured medium with fractures modeled by the surfaces of discontinuity of displacements: J. Math. Sci., **86**, 2735–2746.

Nichols, D., Muir, F., and Schoenberg, M., 1989, Elastic properties of rocks with multiple sets of fractures: 59th Ann. Internat. Mtg., Soc. Expl. Geophys., Expanded Abstracts, 471–474.

Rüger, A., 1997, *P*-wave reflection coefficients for transversely isotropic models with vertical and horizontal axis of symmetry: Geophysics, **62**, 713–722.

——— 1998, Variation of *P*-wave reflectivity with offset and azimuth in anisotropic media: Geophysics, **63**, 935–947.

Schoenberg, M., 1980, Elastic wave behavior across linear slip interfaces: J. Acoust. Soc. Am., **68**, 1516–1521.

——— 1983, Reflection of elastic waves from periodically stratified media with interfacial slip: Geophys. Prosp., **31**, 265–292.

Schoenberg, M., and Douma, J., 1988, Elastic wave propagation in media with parallel fractures and aligned cracks: Geophys. Prosp., **36**, 571–590.

Schoenberg, M., and Helbig, K., 1997, Orthorhombic media: Modeling elastic wave behavior in a vertically fractured earth: Geophysics, **62**, 1954–1974.

Schoenberg, M., and Muir, F., 1989, A calculus for finely layered anisotropic media: Geophysics, **54**, 581–589.

Schoenberg, M., and Sayers, C., 1995, Seismic anisotropy of fractured rock: Geophysics, **60**, 204–211.

Thomsen, L., 1986, Weak elastic anisotropy: Geophysics, **51**, 1954–1966.

——— 1995, Elastic anisotropy due to aligned cracks in porous rock: Geophys. Prosp., **43**, 805–830.

Tsvankin, I., 1997a, Reflection moveout and parameter estimation for horizontal transverse isotropy: Geophysics, **62**, 614–629.

——— 1997b, Anisotropic parameters and *P*-wave velocity for orthorhombic media: Geophysics, **62**, 1292–1309.

Winterstein, D. F., 1990, Velocity anisotropy terminology for geophysicists: Geophysics, **55**, 1070–1088.

APPENDIX A

COMPLIANCE FORMALISM FOR FRACTURED MEDIA

Here we review both exact and approximate methods of obtaining effective parameters of fractured media using the results of Schoenberg (1980, 1983), Schoenberg and Douma (1988), Schoenberg and Muir (1989), Nichols et al. (1989), and Molotkov and Bakulin (1997). A discussion of different approaches to effective medium theory for fractured models can be found in part I.

To simplify the derivation of the effective elastic parameters of fractured media, it is convenient to use the compliances **s** instead of the stiffnesses **c**. The effective compliance matrix of a fractured medium can be written as the sum of the background compliance $\mathbf{s}_b$ and the so-called matrix of excess fracture compliance $\mathbf{s}_f$:

$$\mathbf{c}^{-1} \equiv \mathbf{s} = \mathbf{s}_b + \mathbf{s}_f. \tag{A-1}$$

If the background is VTI, then the stiffness matrix is given by

$$\mathbf{c}_b \equiv \mathbf{s}_b^{-1} = \begin{pmatrix} c_{11b} & c_{12b} & c_{13b} & 0 & 0 & 0 \\ c_{12b} & c_{11b} & c_{13b} & 0 & 0 & 0 \\ c_{13b} & c_{13b} & c_{33b} & 0 & 0 & 0 \\ 0 & 0 & 0 & c_{44b} & 0 & 0 \\ 0 & 0 & 0 & 0 & c_{44b} & 0 \\ 0 & 0 & 0 & 0 & 0 & c_{66b} \end{pmatrix}, \tag{A-2}$$

where $c_{12b} = c_{11b} - 2c_{66b}$. The matrix $\mathbf{s}_f$ of the excess compliance of a fracture set with the normal in the x_1-direction can be written as

$$\mathbf{s}_f = \begin{pmatrix} K_N & 0 & 0 & 0 & 0 & 0 \\ 0 & 0 & 0 & 0 & 0 & 0 \\ 0 & 0 & 0 & 0 & 0 & 0 \\ 0 & 0 & 0 & 0 & 0 & 0 \\ 0 & 0 & 0 & 0 & K_V & 0 \\ 0 & 0 & 0 & 0 & 0 & K_H \end{pmatrix}, \tag{A-3}$$

where K_N is the normal fracture compliance and K_V and K_H are the two shear compliances in the vertical and horizontal directions. The matrix $\mathbf{s}_f$ is no longer diagonal if the fractures are corrugated (part I; for more details, see part III of this series). Since $K_V \neq K_H$, fractures described by matrix (A-3) are sometimes called orthorhombic (Schoenberg and Douma, 1988).

It is convenient to replace the excess fracture compliances K_N, K_V, and K_H by the following dimensionless quantities introduced by Schoenberg and Helbig (1997):

$$\Delta_N = \frac{K_N c_{11b}}{1 + K_N c_{11b}}, \quad \Delta_V = \frac{K_V c_{44b}}{1 + K_V c_{44b}}, \quad \Delta_H = \frac{K_H c_{66b}}{1 + K_H c_{66b}}. \tag{A-4}$$

Then equation (A-3) becomes

$$\mathbf{s}_f = \begin{pmatrix} \dfrac{\Delta_N}{c_{11b}(1-\Delta_N)} & 0 & 0 & 0 & 0 & 0 \\ 0 & 0 & 0 & 0 & 0 & 0 \\ 0 & 0 & 0 & 0 & 0 & 0 \\ 0 & 0 & 0 & 0 & 0 & 0 \\ 0 & 0 & 0 & 0 & \dfrac{\Delta_V}{c_{44b}(1-\Delta_V)} & 0 \\ 0 & 0 & 0 & 0 & 0 & \dfrac{\Delta_H}{c_{66b}(1-\Delta_H)} \end{pmatrix}. \tag{A-5}$$

We call Δ_N, Δ_V, and Δ_H the normal, vertical, and horizontal weaknesses introduced by the fractures (Bakulin and Molotkov, 1998). The weaknesses vary from 0 to 1, with the zero value corresponding to unfractured media and unity describing heavily fractured media in which the P- (for $\Delta_N = 1$) or S-wave (for $\Delta_V = 1$ or $\Delta_H = 1$) velocity vanishes for propagation across the fractures (part I).

Substituting equations (A-2) and (A-5) into equation (A-1) yields the effective stiffness matrix for a single fracture set embedded in a VTI background (Schoenberg and Helbig, 1997):

$$\mathbf{c} = \begin{pmatrix} \tilde{\mathbf{c}}_1 & \mathbf{0} \\ \mathbf{0} & \tilde{\mathbf{c}}_2 \end{pmatrix}, \tag{A-6}$$

where

$$\tilde{\mathbf{c}}_1 = \begin{pmatrix} c_{11_b}(1-\Delta_N) & c_{12_b}(1-\Delta_N) & c_{13_b}(1-\Delta_N) \\ c_{12_b}(1-\Delta_N) & c_{11_b} - \Delta_N \dfrac{c_{12_b}^2}{c_{11_b}} & c_{13_b}\left(1-\Delta_N \dfrac{c_{12_b}}{c_{11_b}}\right) \\ c_{13_b}(1-\Delta_N) & c_{13_b}\left(1-\Delta_N \dfrac{c_{12_b}}{c_{11_b}}\right) & c_{33_b} - \Delta_N \dfrac{c_{13_b}^2}{c_{11_b}} \end{pmatrix}, \tag{A-7}$$

$$\tilde{\mathbf{c}}_2 = \begin{pmatrix} c_{44b} & 0 & 0 \\ 0 & c_{44b}(1-\Delta_V) & 0 \\ 0 & 0 & c_{66b}(1-\Delta_H) \end{pmatrix}, \tag{A-8}$$

and $\mathbf{0}$ is the 3×3 zero matrix.

Alternatively, the same result can be obtained using the series

$$\mathbf{c} \equiv [\mathbf{s}_b + \mathbf{s}_f]^{-1} = \left[\left(\mathbf{I} + \mathbf{s}_f \mathbf{s}_b{}^{-1}\right)\mathbf{s}_b\right]^{-1} = \mathbf{c}_b[\mathbf{I} + \mathbf{s}_f \mathbf{c}_b]^{-1} = \mathbf{c}_b \sum_{k=0}^{\infty} (-\mathbf{s}_f \mathbf{c}_b)^k, \tag{A-9}$$

where $\mathbf{I}$ is the 6×6 identity matrix. Series (A-9) converges to equation (A-6) if all eigenvalues of the matrix $\mathbf{s}_f \mathbf{c}_b$ have absolute values less than 1. This is always the case if the weaknesses Δ_N, Δ_V, and Δ_H, which define nonzero eigenvalues of the matrix $\mathbf{s}_f$ [see equation (A-5)], are sufficiently small.

Equation (A-9) can serve as the basis for developing useful approximations for the effective stiffness matrix $\mathbf{c}$. If the crack density (or fracture intensity) is small and the weaknesses $\{\Delta_N, \Delta_V, \Delta_H\} \ll 1$, we may truncate series (A-9) by keeping only linear terms with respect to Δ_N, Δ_V, and Δ_H:

$$\mathbf{c} \approx \mathbf{c}_b - \mathbf{c}_b \mathbf{s}_f \mathbf{c}_b. \tag{A-10}$$

It is interesting to note that equation (A-10) becomes exact if we replace the matrix $\mathbf{s}_f$ [equation (A-5)] by its linearized version:

$$\mathbf{s}_f^{\text{lin}} = \begin{pmatrix} \Delta_N / c_{11_b} & 0 & 0 & 0 & 0 & 0 \\ 0 & 0 & 0 & 0 & 0 & 0 \\ 0 & 0 & 0 & 0 & 0 & 0 \\ 0 & 0 & 0 & 0 & 0 & 0 \\ 0 & 0 & 0 & 0 & \Delta_V / c_{44_b} & 0 \\ 0 & 0 & 0 & 0 & 0 & \Delta_H / c_{66_b} \end{pmatrix}. \tag{A-11}$$

Approximation (A-10) can be used to obtain two important results. First, it can be extended in a straightforward way to multiple fracture sets (Nichols et al., 1989). If the effective compliance represents the sum of the excess compliances of N fracture sets,

$$\mathbf{s}_f = \sum_{i=1}^{N} \mathbf{s}_{fi}, \tag{A-12}$$

then for the effective stiffness $\mathbf{c}$ we have from equation (A-10)

$$\mathbf{c} \approx \mathbf{c}_b - \sum_{i=1}^{N} \mathbf{c}_b \mathbf{s}_{fi} \mathbf{c}_b. \tag{A-13}$$

The compliance matrix $\mathbf{s}_{fi}$ cannot be described by equation (A-3) if the normal $\mathbf{n}_i$ to the ith fracture set does not coincide with the x_1-axis. The matrices $\mathbf{s}_{fi}$ for arbitrary orientation of $\mathbf{n}_i$ may be obtained from equation (A-3) using the so-called Bond rotation (Winterstein, 1990). For example, the compliance matrix for a fracture set with the normal $\mathbf{n}_i = [0, 1, 0]$ has the form

$$\mathbf{s}_{fi} = \begin{pmatrix} 0 & 0 & 0 & 0 & 0 & 0 \\ 0 & K_N & 0 & 0 & 0 & 0 \\ 0 & 0 & 0 & 0 & 0 & 0 \\ 0 & 0 & 0 & K_V & 0 & 0 \\ 0 & 0 & 0 & 0 & 0 & 0 \\ 0 & 0 & 0 & 0 & 0 & K_H \end{pmatrix}. \tag{A-14}$$

Second, equation (A-10) is well suited for deriving the weak-anisotropy approximation for the stiffnesses of effective media formed by fractures embedded in an anisotropic background. We assume that the background medium is weakly anisotropic, so that

$$\mathbf{c}_b = \mathbf{c}_b^{\text{iso}} + \varepsilon \mathbf{c}_b^{\text{ani}}, \tag{A-15}$$

where $\mathbf{c}_b^{\text{iso}}$ is the stiffness matrix of a purely isotropic solid that approximates $\mathbf{c}_b$ in some sense, $\mathbf{c}_b^{\text{ani}}$ is the anisotropic portion

of $\mathbf{c}_b$, and $\varepsilon \ll 1$. We also assume that the elements of the fracture compliance matrix are of the same order as ε and can be denoted as $\varepsilon \mathbf{s}_f$. If we represent the effective stiffness matrix $\mathbf{c}$ in a form similar to equation (A-15), equation (A-10) can be rewritten as

$$\mathbf{c}^{\text{iso}} + \varepsilon \mathbf{c}^{\text{ani}} \approx \mathbf{c}_b^{\text{iso}} + \varepsilon \mathbf{c}_b^{\text{ani}} - \left(\mathbf{c}_b^{\text{iso}} + \varepsilon \mathbf{c}_b^{\text{ani}}\right) \varepsilon \mathbf{s}_f \left(\mathbf{c}_b^{\text{iso}} + \varepsilon \mathbf{c}_b^{\text{ani}}\right). \tag{A-16}$$

Collecting the terms linear in ε yields

$$\mathbf{c}^{\text{ani}} = \mathbf{c}_b^{\text{ani}} - \mathbf{c}_b^{\text{iso}} \mathbf{s}_f \mathbf{c}_b^{\text{iso}}. \tag{A-17}$$

This equation, valid in the weak anisotropy limit, can be loosely interpreted in the following way: the anisotropy $\mathbf{c}^{\text{ani}}$ of an effective medium containing fractures in an anisotropic background described by $\mathbf{c}_b$ is equal to the sum of the background anisotropy $\mathbf{c}_b^{\text{ani}}$ and the anisotropy caused by the fractures embedded into any isotropic medium with $\mathbf{c}_b^{\text{iso}}$ sufficiently close to $\mathbf{c}_b$ [see equation (A-13)]. The matrix $\mathbf{c}_b^{\text{iso}}$ must satisfy the inequality $|(||\mathbf{c}_b||/||\mathbf{c}_b^{\text{iso}}||) - 1| < \varepsilon$.

APPENDIX B

ANISOTROPIC PARAMETERS FOR ORTHORHOMBIC MEDIA

The basic set of the anisotropic parameters for orthorhombic media has been introduced by Tsvankin (1997b). His notation contains the vertical velocities of the P-wave and one of the S-waves and seven dimensionless Thomsen-type (1986) anisotropic coefficients. The definitions of those parameters in terms of the stiffnesses c_{ij} and density ρ are given below.

V_{P0}—the P-wave vertical velocity:

$$V_{P0} \equiv \sqrt{\frac{c_{33}}{\rho}} \qquad (\rho \text{ is density}). \tag{B-1}$$

V_{S0}—the velocity of the vertically traveling S-wave polarized in the x_1-direction:

$$V_{S0} \equiv \sqrt{\frac{c_{55}}{\rho}}. \tag{B-2}$$

$\epsilon^{(2)}$—the VTI parameter ϵ in the $[x_1, x_3]$ symmetry plane normal to the x_2-axis [this explains the superscript (2)]:

$$\epsilon^{(2)} \equiv \frac{c_{11} - c_{33}}{2c_{33}}. \tag{B-3}$$

$\delta^{(2)}$—the VTI parameter δ in the $[x_1, x_3]$ plane:

$$\delta^{(2)} \equiv \frac{(c_{13} + c_{55})^2 - (c_{33} - c_{55})^2}{2c_{33}(c_{33} - c_{55})}. \tag{B-4}$$

$\gamma^{(2)}$—the VTI parameter γ in the $[x_1, x_3]$ plane:

$$\gamma^{(2)} \equiv \frac{c_{66} - c_{44}}{2c_{44}}. \tag{B-5}$$

$\epsilon^{(1)}$—the VTI parameter ϵ in the $[x_2, x_3]$ symmetry plane:

$$\epsilon^{(1)} \equiv \frac{c_{22} - c_{33}}{2c_{33}}. \tag{B-6}$$

$\delta^{(1)}$—the VTI parameter δ in the $[x_2, x_3]$ plane:

$$\delta^{(1)} \equiv \frac{(c_{23} + c_{44})^2 - (c_{33} - c_{44})^2}{2c_{33}(c_{33} - c_{44})}. \tag{B-7}$$

$\gamma^{(1)}$—the VTI parameter γ in the $[x_2, x_3]$ plane:

$$\gamma^{(1)} \equiv \frac{c_{66} - c_{55}}{2c_{55}}. \tag{B-8}$$

$\delta^{(3)}$—the VTI parameter δ in the $[x_1, x_2]$ plane (x_1 plays the role of the symmetry axis):

$$\delta^{(3)} \equiv \frac{(c_{12} + c_{66})^2 - (c_{11} - c_{66})^2}{2c_{11}(c_{11} - c_{66})}. \tag{B-9}$$

These nine parameters fully describe wave propagation in general orthorhombic media. In particular applications, however, it is convenient to operate with specific combinations of Tsvankin's parameters. For example, P-wave NMO velocity from dipping reflectors depends on three coefficients η, which determine the anellipticity of the P-wave slowness in the symmetry planes (Grechka and Tsvankin, 1999). The definitions of $\eta^{(1,2,3)}$ are analogous to that of the Alkhalifah–Tsvankin (1995) coefficient η in VTI media:

$\eta^{(1)}$—the VTI parameter η in the $[x_2, x_3]$ plane:

$$\eta^{(1)} \equiv \frac{\epsilon^{(1)} - \delta^{(1)}}{1 + 2\delta^{(1)}}. \tag{B-10}$$

$\eta^{(2)}$—the VTI parameter η in the $[x_1, x_3]$ plane:

$$\eta^{(2)} \equiv \frac{\epsilon^{(2)} - \delta^{(2)}}{1 + 2\delta^{(2)}}. \tag{B-11}$$

$\eta^{(3)}$—the VTI parameter η in the $[x_1, x_2]$ plane:

$$\eta^{(3)} \equiv \frac{\epsilon^{(1)} - \epsilon^{(2)} - \delta^{(3)}\left(1 + 2\epsilon^{(2)}\right)}{\left(1 + 2\epsilon^{(2)}\right)\left(1 + 2\delta^{(3)}\right)}. \tag{B-12}$$

Vertical transverse isotropy may be considered as a special case of orthorhombic media, where

$$\epsilon^{(1)} = \epsilon^{(2)} = \epsilon, \tag{B-13}$$

$$\delta^{(1)} = \delta^{(2)} = \delta, \tag{B-14}$$

$$\gamma^{(1)} = \gamma^{(2)} = \gamma, \tag{B-15}$$

$$\delta^{(3)} = 0, \tag{B-16}$$

and, as a consequence,

$$\eta^{(1)} = \eta^{(2)} = \eta, \tag{B-17}$$

$$\eta^{(3)} = 0. \tag{B-18}$$

APPENDIX C

TWO IDENTICAL FRACTURE SETS

If the model includes two identical orthogonal fracture sets in a purely isotropic background, only four effective stiffnesses out of nine remain independent because the stiffness matrix depends on just four quantities: λ, μ, $\Delta_{N1}=\Delta_{N2}\equiv\Delta_N$, and $\Delta_{T1}=\Delta_{T2}\equiv\Delta_T$. From equations (40)–(43) it follows that in this case $c_{11}=c_{22}$, $c_{13}=c_{23}$, and $c_{44}=c_{55}$. Constraints (47) and (48) become identical and, together with equation (46), may be reduced to

$$c_{12}(c_{33}+c_{13})=c_{13}(c_{11}+c_{13}) \tag{C-1}$$

and

$$2(c_{11}+c_{13})c_{44}c_{66}=(2c_{66}-c_{44})\left(c_{11}c_{33}-c_{13}^2\right). \tag{C-2}$$

We can call this medium quasi-VTI because its stiffness matrix is close to the one for vertical transverse isotropy. Unlike real VTI media, however, the stiffnesses of the quasi-VTI model satisfy constraints (C-1) and (C-2), which replace the VTI relationship $c_{11}=c_{12}+2c_{66}$. Indeed, the combination of the stiffnesses that must vanish in VTI media can be written in the exact form as

$$c_{11}-2c_{66}-c_{12}=\frac{4\mu^2(K_T-K_N)}{(1+2\mu K_N)(1+2\,\mu K_T)}. \tag{C-3}$$

Hence, because of the difference between the normal and shear compliances, the model with two identical fracture sets does not have the VTI symmetry.

The anisotropic coefficients of quasi-VTI media are described by equations (B-3)–(B-5), (B-13)–(B-15), and

$$\begin{aligned}\delta^{(3)}=&-\left[\frac{4\mu^2(\lambda+\mu)(K_T-K_N)}{2\mu+\dfrac{\lambda}{1+2(\lambda+\mu)K_N}}\right]\\&\times\left[\mu+2\mu(\lambda+\mu)(K_T-K_N)+\frac{\lambda(1+4\mu K_N)}{1+2\mu K_N}\right.\\&\left.+2\mu^2K_T\frac{1+2(\lambda+\mu)K_N}{1+2\mu K_N}\right]^{-1}.\end{aligned} \tag{C-4}$$

Interestingly, quasi-VTI media have two additional vertical symmetry planes at 45° with respect to planes $[x_1, x_3]$ and $[x_2, x_3]$. Clearly, expressions for anisotropic coefficients $\epsilon^{(1,2)}$, $\delta^{(1,2)}$, and $\gamma^{(1,2)}$, which could be defined within these symmetry planes, are different from those given by equations (49)–(58).

Two identical scalar fracture sets

If we further assume that both fracture sets are filled with gas [i.e., $K_N=K_T$; Schoenberg and Sayers (1995); part I], the effective medium becomes VTI. The effective stiffnesses given below depend only on the background parameters λ and μ and the weakness $\Delta_T=(K_T\mu)/(1+K_T\mu)$ [equation (45)]:

$$c_{11}=(\lambda+2\mu)\frac{(1-\Delta_T)[1+\Delta_T(3-4g)]}{D}, \tag{C-5}$$

$$c_{13}=\lambda\frac{1-\Delta_T^2}{D}, \tag{C-6}$$

$$c_{33}=(\lambda+2\mu)\frac{1-\Delta_T(8g-5)}{D}, \tag{C-7}$$

$$c_{44}=\mu(1-\Delta_T), \tag{C-8}$$

$$c_{66}=\mu\frac{1-\Delta_T}{1+\Delta_T}, \tag{C-9}$$

where

$$D\equiv(1+\Delta_T)[1+\Delta_T(2-3g)]. \tag{C-10}$$

The five stiffness elements of this three-parameter VTI medium are related by two constraints that can be obtained by substituting the VTI relation $c_{11}=c_{12}+2c_{66}$ into equations (C-1) and (C-2). In terms of Thomsen's (1986) anisotropic coefficients, these constraints take the form

$$\epsilon=\delta=4\gamma(1+2\gamma)(1-g). \tag{C-11}$$

The equality $\epsilon=\delta$ indicates that the effective medium is elliptically anisotropic. In the weak-anisotropy limit, equation (C-11) yields

$$\epsilon=\delta\approx4\gamma(1-g). \tag{C-12}$$

For a typical value $g=0.25$, $\epsilon=\delta\approx3\gamma$.

APPENDIX D

FRACTURE CHARACTERIZATION FOR TWO ORTHOGONAL FRACTURE SETS: SPECIAL CASES

Azimuthally independent *P*-wave NMO velocity

In contrast to the case of a single fracture set in an isotropic or VTI background, the orientation of two orthogonal fracture systems cannot always be found from the *P*-wave NMO ellipse from a horizontal reflector. If $\delta^{(1)}=\delta^{(2)}$ or, equivalently,

$$(1-2g)\Delta_{N1}+\Delta_{T1}=(1-2g)\Delta_{N2}+\Delta_{T2} \tag{D-1}$$

[equations (50) and (54)], the *P*-wave NMO ellipse degenerates into a circle. This equation does not necessarily imply that the two systems of fractures are identical because it can be satisfied for fracture sets with different crack densities (e.g., $\Delta_{T1}>\Delta_{T2}$) and different fluid saturations ($\Delta_{N1}<\Delta_{N2}$). The azimuths of fractures in this case can be found from the shear-wave polarization directions or by using *P*-wave reflections from dipping interfaces and/or the azimuthal variation of *P*-wave nonhyperbolic moveout.

Equal tangential weaknesses

If the tangential weaknesses are equal to each other ($\Delta_{T1}=\Delta_{T2}$), the anisotropic coefficients $\gamma^{(1)}$ and $\gamma^{(2)}$ also become identical [see equations (51) and (55)] and there is no shear-wave splitting at vertical incidence. Hence, the fracture orientation cannot be determined from shear-wave splitting. However, if the fracture sets have different normal weaknesses ($\Delta_{N1}\neq\Delta_{N2}$), the fracture azimuths can be found using *P*-wave NMO ellipses from a horizontal or a dipping reflector.

Identical fracture sets (quasi-VTI medium)

In the case of two identical orthogonal fracture sets, neither the P-wave NMO ellipse from a horizontal reflector (it degenerates into a circle because $\delta^{(1)} = \delta^{(2)}$) nor the shear-wave polarization directions ($\gamma^{(1)} = \gamma^{(2)}$, see Appendix C) can be used to detect the fracture orientation. Still, since $\delta^{(3)}$ (or $\eta^{(3)}$) differs from zero, the orientation can be found from normal moveout of dipping P events or from P-wave nonhyperbolic moveout. The rest of the inversion procedure is similar to that for the general case of two different fracture systems.

Despite the absence of shear-wave splitting in the vertical direction, S-waves can still be used for estimating fracture parameters. The wavefront of the slow shear wave in quasi-VTI media always has cusps at 45° with respect to the symmetry planes $[x_1, x_3]$ and $[x_2, x_3]$ (Figure D-1) if $c_{11} - 2c_{66} - c_{12} > 0$ [or, equivalently, $K_T > K_N$; see equation (C-3) and part I]. This wavefront structure by itself can be used to identify the symmetry directions (and, therefore, the fracture strikes) if a sufficient number of azimuthal measurements is available. Once those directions are found, we can use equations (23)–(29) for the NMO velocities of the S_1- and S_2-waves in the vertical symmetry planes and estimate the fracture parameters based on equations (66) and (68). It is interesting that in quasi-VTI media the S-wave NMO velocities from a horizontal reflector are defined, strictly speaking, *only* within the vertical symmetry planes because the shear-wave singularity makes the S-wave offset-traveltime curve nondifferentiable in any other azimuth.

Identical gas-filled fracture sets (VTI medium)

Finally, if two identical fracture sets are gas filled, the effective medium becomes VTI (Appendix C). Since the VTI model is azimuthally isotropic, it is impossible to find the fracture orientation from seismic data. The single parameter Δ_T (or K_T) needed to describe the fractures can be found from any anisotropic coefficient given by equations (49)–(56) if the background V_S/V_P ratio is known. Estimating several anisotropic coefficients provides a redundancy that can be used to verify the validity of this model [see equation (C-11)]. Indeed, this VTI medium is elliptical ($\epsilon = \delta$) and has a specific relationship (C-12) between ϵ and γ.

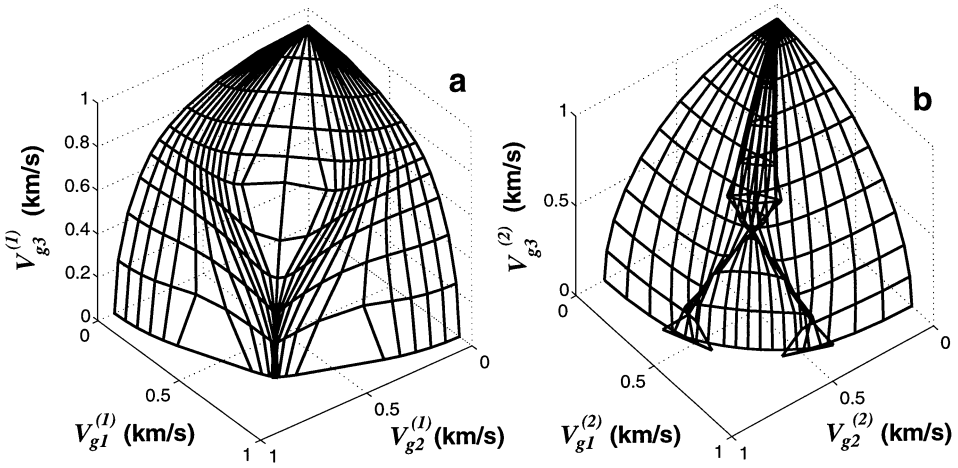

FIG. D-1. Group velocity surfaces of the (a) fast and (b) slow shear waves for the model with two identical orthogonal fracture sets. The background velocities are $V_P = 2$ km/s and $V_S = 1$ km/s. The fracture weaknesses $\Delta_N = 0$ and $\Delta_T = 0.15$ approximately correspond to fluid-filled penny-shaped cracks with a crack density of 7%.